High Power Arbitrary RF Pulse Shaping Tests with NG-LLRF and Cool Copper Collider Prototype Structure

Chao Liu^{1,*}, Ankur Dhar¹, Ronald Agustsson², Diego Amirari², Dennis Palmer¹, Martin Breidenbach¹, and Emilio Nanni¹

¹SLAC National Accelerator Laboratory, Menlo Park, California, USA

Abstract. RF pulse modulation techniques are widely applied to shape RF pulses for various types of RF stations of particle accelerators. The amplitude and phase modulations are typically implemented with additional RF components that require drive or control electronics. For the RF system-on-chip (RF-SoC) based next generation LLRF (NG-LLRF) platform, which we have developed in the last several years, RF modulation and demodulation are fully implemented in the digital domain. Therefore, arbitrary RF pulse shaping can be realized without any additional analogue components. We performed a range of high-power experiments with the NG-LLRF and a prototype Cool Copper Collider (C³) structure. In this paper, the RF field measured at different stages with different pulse shapes and peak power levels up to 16.45 MW will be demonstrated and analyzed. The high precision pulse shaping schemes of the NG-LLRF can be applied to realize the phase modulation for a linear accelerator injector, the phase reversal for a pulse compressor, or the modulation required to compensate for the beam loading effect.

1 Introduction

The low-level radio frequency (LLRF) systems for particle accelerators typically stabilize the electromagnetic field in accelerator cavities with extremely high precision to achieve the optimum beam quality. As accelerator technology advances, the functional requirements for the LLRF have been extended. From single bunch per RF pulse to multiple bunch, the requirement of controlling the stability within each RF pulse has been added to the pulse-to-pulse stability control. More aggressively, new accelerator concepts, such as programmable accelerators, have been proposed that will require the LLRF to deliver RF pulses with an arbitrary envelope with extremely high precision. With the programmable accelerator, the charge, beam energy, repetition rate, and other operation parameters can be rapidly tuned in real-time. The enormous flexibility of operation can enable for more sustainable, more adaptable, and potentially more ground breaking high-energy physics experiments.

The RF system-on-chip (RFSoC) based next generation LLRF (NG-LLRF) system we were developing over the last several years employs direct RF sampling technology. NG-LLRF generates and samples the RF signals directly, and all up and down conversions are

²RadiaBeam Technologies LLC, Santa Monica, USA

^{*}e-mail: chaoliu@slac.stanford.edu. This article will be submitted as proceedings for the 2025 International Workshop on Future Linear Colliders (LCWS2025).

implemented in the digital domain. The conversions are implemented with the hardened numerical controlled oscillators (NCOs) in RFSoC. Arbitrary pulse shapes could be modulated with the NCO output, and the integrated high-speed DAC synthesizes the RF pulses directly.

The direct RF sampling technique can significantly simplify the analogue RF circuit compared with the heterodyne-based system architecture, but the RF performance of the sampling technique was the major concern for our targeted applications. Since RFSoC has been released in 2018, we have investigated the continuous-wave (CW) RF performance of the RFSoC data converters in different frequency ranges and developed receiver and readout platforms for various physics experiments [1–6]. The RFSoC demonstrated high RF stability in CW test setups[1, 3], but a range of particle accelerators operate with RF pulses. Therefore, we have conducted a variety of pulse-to-pulse stability studies for C-band [7–11] and S-band LLRF systems for accelerators [12]. We have designed the first LLRF prototype for our initial target application, the new proposed lepton collider Higgs factory, Cool Copper Collider (C³ or CCC). The prototype demonstrated around 80 femtoseconds (fs) [10] phase jitter with a direct loopback and the 150 fs requirement of C³ [13] is highly achievable with the NG-LLRF platform. In [14], NG-LLRF has been identified as the LLRF solution for C³. In this paper, we will present a feasibility study of scaling up the NG-LLRF for the full C³ from architectural and cost perspectives.

As introduced in [10], we performed preliminary high-power tests with C^3 accelerating structure cavities using the test facility at Radiabeam. The prototype C^3 structure was also driven by RF pulses with different modulation schemes with potential applications at different types of accelerator RF station. In this paper, the measurement results with square modulation and alternative modulations will be compared to demonstrate the flexibility of the NG-LLRF in arbitrary pulse shaping.

2 Scaling up NG-LLRF for Cool Copper Collider

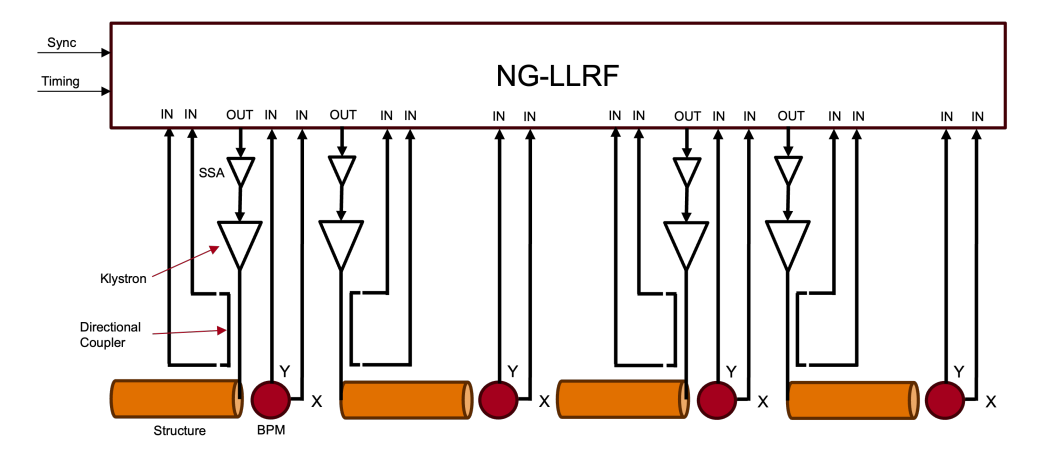


Figure 1: The conceptual block diagram of a single NG-LLRF module for C³. The NG-LLRF system has 16 RF inputs and 16 outputs. All the RF inputs are utilized and only 4 of the RF outputs are used to drive the 4 accelerators for half of a cryo-module.

Figure 1 shows the conceptual design of an NG-LLRF module for C³ linear accelerators (LINACs). The NG-LLRF is designed to be synchronized with the RF reference and is triggered by the accelerator timing system. We are working on more detailed designs of

Table 1: System breakdown of the C³

System Level	Number of systems
LINACs	2
Cryomodules	275
Rafts	4
Accelerators	2
RF inputs	4
RF outputs	1

the synchronization and timing systems considering scaling up for the entire collider. Considering the high density of the RF input and output channels of C³ accelerating structure, the RFSoC device with 16 ADCs and 16 DACs has been identified as the base platform of NG-LLRF for it. Each NG-LLRF module can drive and monitor 4 accelerators. For each of the accelerator, there are 4 RF signals, which are forward and reflection couplers from an accelerating structure, and the two RF signals from the beam position monitor for each structure. Based on each pair of forward and reflection RF pulses directly sampled by the integrated ADCs in RFSoC, an updated RF pulse will be computed in firmware and a DAC will synthesize the new RF pulse directly. In [8, 9], the architecture of feedback loop designs is described in more detail.

In Table 1, the breakdown of the subsystems at different levels of C³ is summarized. Based on these statistics, the LLRF system of C³ requires 17,600 RF inputs and 4,400 RF outputs in total. Therefore, around 1,100 NG-LLRF modules will be required for the entire collider. The estimated cost of an NG-LLRF module is currently around \$ 20k. For each module, we will be using 16 inputs and 4 outputs from each of the NG-LLRF channels. Therefore, the estimated cost per RF channel is around \$ 1k, which is cost-effective compared to the conventional LLRF system. The total cost of the LLRF system will be approximately \$ 22M excluding the timing and synchronization systems and cable networks.

3 High-Power Test of NG-LLRF with Cool Copper Collider Prototype Accelerating Structure with Different RF Pulse Shapes

3.1 High-power Test Setup

The high-power test was performed with a C-band high-power test stand and the test setup schematics is shown in Figure 2. RF pulses are synthesized directly by an integrated DAC in the RFSoC device of the NG-LLRF. A baseband pulse is loaded into the FPGA from the server via the GbE link. Then the baseband pulse is interpolated and up converted with a digital mixer. The DAC decodes the digital samples and is synthesized by an integrated DAC. In this test, the NG-LLRF generates the RF pulse with frequency around 5.712 GHz and the RF pulse feeds to a solid state amplifier (SSA) to drive the klystron. RF power is injected to the C³ prototype structure. There are couplers at three stages of the test setup, the klystron forward, the cavity forward, and cavity reflection. The RF signals from the couplers are attenuated and looped back to NG-LLRF. The three RF pulse are directly sampled by the integrated ADCs in the fifth-order Nyquist. The digital samples are down converted with digital mixer at the corresponding RF frequency and then filtered and decimated. The baseband pulses of the three RF channels are recorded for further analysis.

The rated peak power of the test stand is approximately 25 MW with a pulse width of several μ s, but this test was performed before the structure was fully conditioned. In this test,

we have performed tests with two test configurations, 1 μ s pulse width at 10 Hz at 5.2 MW peak power and 500 ns pulse width at 60 Hz at 16.45 MW peak power.

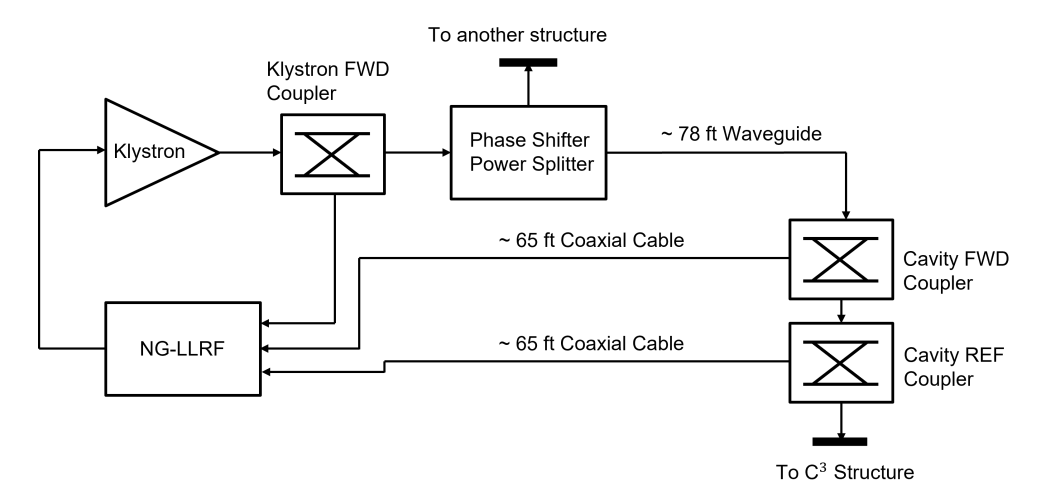


Figure 2: The schematics of high-power test setup for testing the NG-LLRF with C-band high-power test stand and a C³ prototype structure[10].

3.2 RF Pulse with a Linear Phase Ramp

We performed high-power tests with different modulation schemes to evaluate the ability of NG-LLRF to synthesize and measure RF pulses with a variety of pulse shapes. In this test, we used the baseband pulse with a 360 degree linear phase ramp and fixed magnitude over the pulse duration. The peak power injected into the structure for both types of RF pulses is 16.45 MW, pulse width about 500 ns and 60 Hz repetition rate. Figure 3a shows the cavity forward signals with the system driven by RF pulses with square and phase-sweeping modulation schemes. The first peak of the magnitude of the baseband pulse measured with a square pulse drive is scaled to 1 and the scaling factor is used to scale the magnitude of the baseband pulse measured with the other drive. The same scaling scheme will be used for the plots shown in all sections of this article. Due to the cross-coupling of the reflected power to the forward couplers, there are artifacts in both magnitude plots and a more detailed discussion is given in [10]. The phase of the cavity forward signal shows a clear linear phase ramp, which demonstrates that the phase modulation is accurately generated and measured by the NG-LLRF. A 360° linear phase ramp within a 500 ns pulse is equivalent to drive the cavity off resonance by approximately 2 MHz. Therefore, most of the drive power is reflected back, and that explains why the cavity forward and reflection signals have similar profiles.

Figure 3b shows the cavity reflection signals with these two modulation schemes. The magnitude plot of the square wave modulation drive shows a linear decent over the pulse, which shows the field filling process of the structure. The second peak of the magnitude is higher than the first one, which is the desire characteristic of the over-coupling design of the prototype when no beam is presented. When the RF is switched off, the reflections is still far from zero, which indicates that the cavity was not fully filled yet. The linear phase ramp is fully reflected on the phase plot of the cavity reflection with a phase sweep drive.

Similar tests as above were performed with peak power around 5.2 MW peak power, 1 μ s pulse width and 10 Hz repetition rate. In this case, the duration of the 360° linear phase ramp

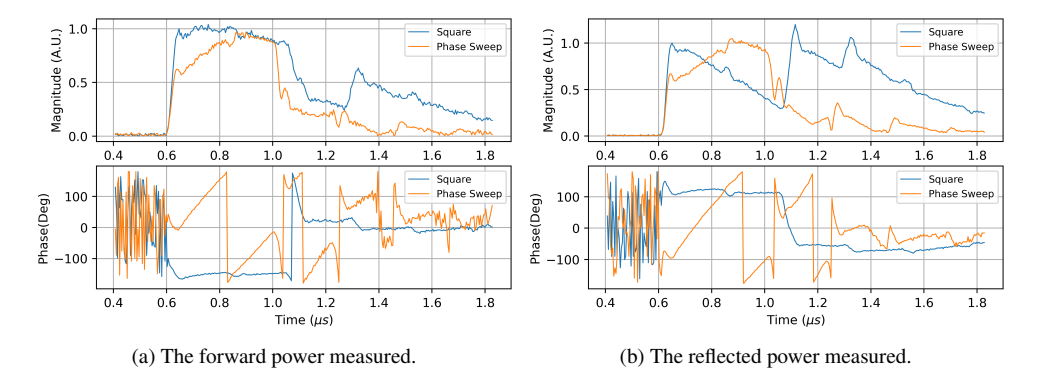


Figure 3: The magnitude and phase of baseband pulses from high power test stand driven by RF pulses modulated with square and linear phase ramp envelope. The pulse width is about 500 ns and the peak power injected to the prototype structure is around 16.45 MW.

has been extended to $1 \mu s$, which can be considered to drive the prototype cavity off resonance by 1 MHz. Figure 4a and 4b show the forward and reflection baseband signals for the square and phase ramp modulation schemes. With this linear phase ramp, the power injected into the structure is also almost fully reflected, since the bandwidth of the cavity structure is on the order of kilohertz. With a 1 μs square pulse, the structure is fully filled in about 700 ns, since the magnitude of the cavity reflection reached zero around that time. After the cavity is fully filled, the magnitude of the reflected signal increases linearly and the phase reversed, as the forward power cannot be filled into the cavity any more and got fully reflected. When the RF is switched off, there is a spike in the reflected signal, which is the desired behavior of an over coupled cavity design, and there is no beam presented in this case.

This test demonstrated that the NG-LLRF is capable of synthesizing and measuring the RF pulses with high precision phase modulation schemes in the C-band without any analog up and down conversions. With flexible phase modulation, phase stabilization within each RF pulse, beam load effect compensation on phase, or other phase modulation schemes that can improve the operation of the accelerating structures or other types of high-power RF stations can be implemented without substantial engineering efforts.

3.3 RF Pulse with Phase Reversals

Phase reversal is a common phase modulation scheme for SLAC Energy Doubler (SLED) type pulse compressors [15]. The prototype C³ structure is not designed for pulse compression, but was tested with RF pulses with phase reversal to demonstrate the capability of the NG-LLRF to generate phase flip. Figure 5a shows the forward coupler measurements with square and phase reversal RF drive modulation schemes with peak power at 16.45 MW. The initial magnitude and phase levels are similar for the two schemes, but a phase flip was successfully generated after 250 ns. Figure 5b shows the reflection signals captured with the two modulation schemes. When the drive phase flipped, the magnitude of the reflected signal reached approximately 2.2 times the initial peak and the phase flipped. That is very similar to a demonstration for the rapid power extraction in the reversed phase of an SLED pulse compressor.

The phase flipping rate has a significant impact on the compression rate of an SLED-based pulse compressor. The phase flipping events at the SSA and klystron output couplers are

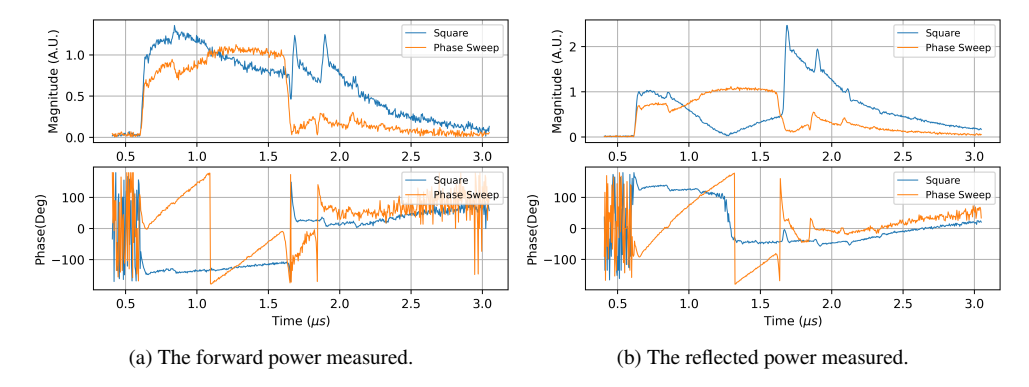


Figure 4: The magnitude and phase of baseband pulses from high power test stand driven by RF pulses modulated with square and linear phase ramp envelope. The pulse width is about $1 \mu s$ and the peak power injected to the prototype structure is around 5.2 MW.

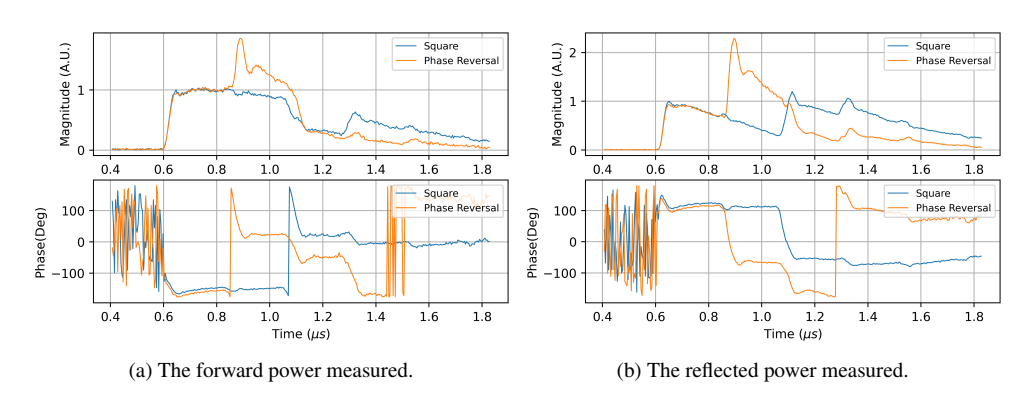


Figure 5: The magnitude and phase of baseband pulses from high power test stand driven by RF pulses modulated with square and square wave with phase reversal every 250 ns envelopes. The pulse width is about 500 ns and the peak power injected to the prototype structure is around 16.45 MW.

shown in Figure 6a and 6a, respectively. The flipping time is often limited by the bandwidth of the RF network. In this case, the flips were accomplished in 4 ns for both couplers. This could be used as a baseline phase flipping rate when we are using NG-LLRF to implement a C-band SLED pulse compressor in the future.

With a 500 ns RF pulse width we can only implement a single phase flipping event. The test was also performed with a 1 μ s pulse with peak power around 5.2 MW and we can realize 3 flips at the same rate. The cavity forward signal shown in Figure 7a demonstrates that the 3 phase flips were successfully generated with the RF network. Figure 7b shows the reflected signals withe two types of drive. The initial phase flip shows the SLED like rapid power extraction and the second flip shows the extraction in reversed phase again. For an SLED-based pulse compressor, the long pulse tail after the desired short pulse can potentially case breakdowns and affect the peak power could be delivered. Therefore, another phase flip

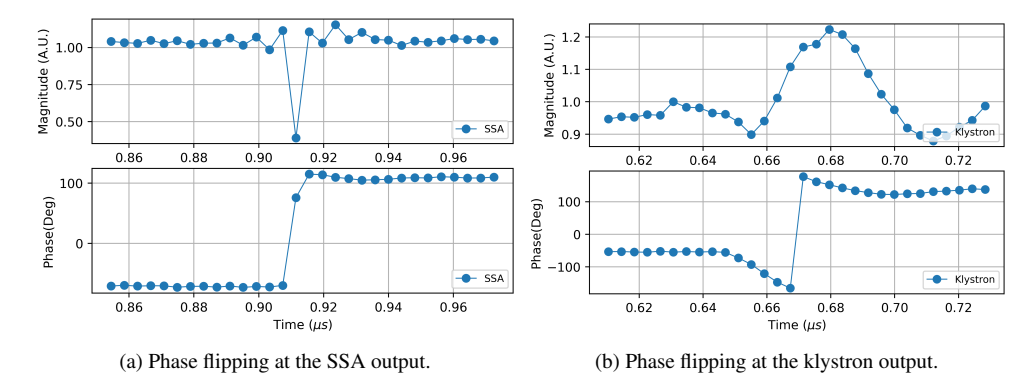


Figure 6: The magnitude and phase measured at SSA and klystron output couplers around the phase flipping event.

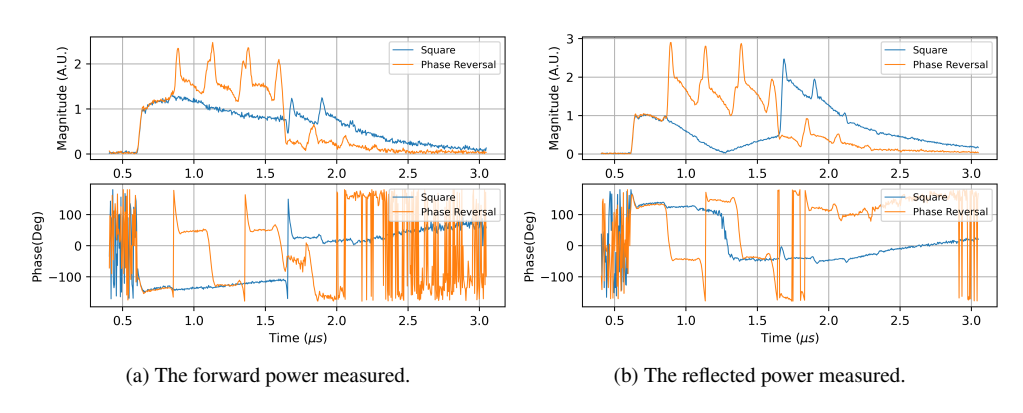


Figure 7: The magnitude and phase of baseband pulses from high power test stand driven by RF pulses modulated with square and square wave with phase reversal every 250 ns envelopes. The pulse width is about 1 μ s and the peak power injected to the prototype structure is around 5.2 MW.

that extracts power rapidly and shortens the pulse tail can help reduce the breakdown rates. That has been demonstrated with the second phase flip in this test. The pulse width can be optimized in future design. This test demonstrates the flexibility of the NG-LLRF platform in phase modulation and it could be the enabling technique for implementing an SLED-based pulse compressor with even high peak power in the future.

3.4 Pulse Train within each RF Pulse

The RF drives with phase modulation schemes were demonstrated in the previous two sections. The test results with an RF drive that has an amplitude modulation, an evenly spaced pulse train, will be described.

Figure 9a shows the forward coupler measurements with square and pulse train modulation. When the RF switched off after the initial 250 ns, the magnitude of the forward RF

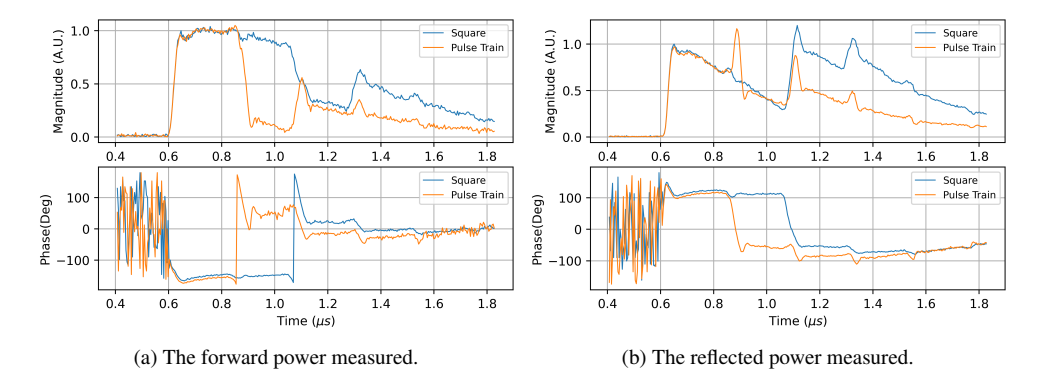


Figure 8: The magnitude and phase of baseband pulses from high power test stand driven by RF pulses modulated with square and pulse train switch on and off every 250 ns envelopes. The pulse width is about 500 ns and the peak power injected to the prototype structure is around 16.45 MW.

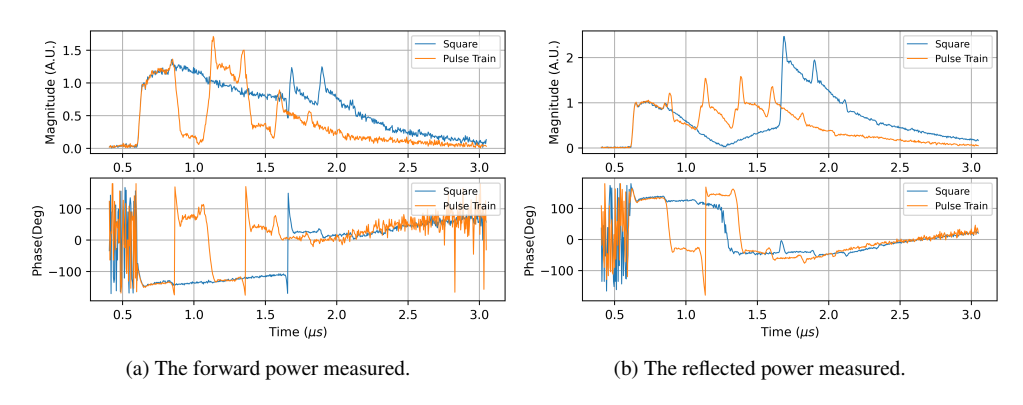


Figure 9: The magnitude and phase of baseband pulses from high power test stand driven by RF pulses modulated with square and pulse train switch on and off every 250 ns envelopes. The pulse width is about 500 ns and the peak power injected to the prototype structure is around 5.2 MW.

measurement does not drop to close to zero as expected. This is the result of cross coupling from reflection to forward, which is discussed in [10]. However, we can see that the amplitude modulation was successfully applied. When the RF is switched off, the peak in the cavity reflection signal with pulse train modulation is lower than that with square modulation, since no RF power filled the structure after 250 ns with pulse train modulation.

The test was also performed with 1 μ s RF pulses with the pulse train modulation at peak power of 5.2 MW. The cavity forward measurements shown in Figure 9a demonstrate that the RF pulse train was successfully generated and delivered to the prototype structure. Figure 9b cavity reflection measurements with the RF drive with two modulation schemes. The field fills and dissipates with the pulse train drive, and the RF power flow can be monitored from the reflection signal.

The pulse train modulation tested in this case is to demonstrate flexible amplitude modulation of the high power RF with an NG-LLRF system. Amplitude modulation can be used for many stations in LINACs. For accelerators operating with bunch trains, the RF field in the structure within is required to be consistent with in each pulse. The RF network and beam loading often introduced uniform distortions to the pulses, and the shape of RF pulses generated by the NG-LLRF need to be tuned to compensate for such effects. The amplitude may also be used for electron bunch generation, such as defining the micro-pulse features and carving out macro-pulses at a variable width.

4 Conclusion

The initial plan for scaling up the NG-LLRF hardware for C³was summarized in this paper. The total cost of the LLRF system for C³ is projected to be \$ 22M, which is \$ 1k per RF channel. Compared with conventional heterodyne based LLRF, the NG-LLRF has a significantly reduced footprint and potentially lower per channel cost, which are primarily because of the elimination of up and down analog RF mixing circuit required by the conventional LLRF for every channel.

We have started prototyping components for C³ and building prototypes stage by stage. In this case, we have summarized a selection of test results from a high-power test with a prototype NG-LLRF and a prototype C³ accelerating structure. The results we focus on in this paper is the test performed using drive RF pulses with different amplitude and phase modulation schemes. For the direct RF synthesizing and sampling technique we adapted for NG-LLRF, the modulation and demonstration are performed fully in the digital domain. Therefore, we can load an arbitrary waveform to the FPGA fabric and get it modulated. Then the integrated DAC decodes the digital samples and synthesizes the RF pulses directly. The integrated ADCs sample the RF signals directly and down-converted the signal to baseband in the digital domain too.

We have tested the system with the RF drive modulated with a linear phase ramp. The test demonstrated the high precision phase modulation capability of the NG-LLRF and the behavior of the prototype C³ structure with an off-resonance drive. Phase flip is also tested with the high-power test stand, as it is an important technique used for SLED-based pulse compressor or other rapid field power extraction applications. The test results demonstrated the rapid power extraction on the reflection signal, which is exactly expected for an SLED structure. The phase flip time with the C-band high power test network measure in this case is below 4 ns, which could be used as a baseline for future C-band pulse compressor design. The bandwidth of the measurement of NG-LLRF is 245.76 MHz, so the resolution of time is about 4 ns. The actual flip time might be even shorter. The system was also tested with an RF drive that has a pulse train pattern. The test results successfully showcased pulse train modulation, which can be adapted for more complex pulse train generation for electron injectors. The modulation schemes tested in this case cover only several commonly used cases and could be extended to arbitrary RF pulse shapes depending on the applications. The high flexible and high precision RF shaping of the NG-LLRF could enable the implementation of the programmable accelerator concept.

5 Acknowledgment

The work of the authors is supported by the U.S. Department of Energy under Contract No. DE-AC02-76SF00515.

References

- [1] C. Liu, M.E. Jones, A.C. Taylor, Characterizing the performance of high-speed data converters for rfsoc-based radio astronomy receivers, Monthly Notices of the Royal Astronomical Society **501**, 5096 (2021).
- [2] C. Liu, M.E. Jones, A.C. Taylor, Development of General-purpose Digital Backend for Single-dish Centimetre and Millimetre-wave Telescopes, in 2022 3rd URSI Atlantic and Asia Pacific Radio Science Meeting (AT-AP-RASC) (IEEE, 2022), pp. 1–4
- [3] C. Liu, L. Ruckman, R. Herbst, Evaluating direct rf sampling performance for rfsoc-based radio-frequency astronomy receivers, arXiv preprint arXiv:2309.08067 (2023).
- [4] S.W. Henderson, Z. Ahmed, J.M. D'Ewart, J.C. Frisch, R. Herbst, C. Liu, L. Ma, L. Ruckman, D.D. Van Winkle, C. Yu, Advanced RFSoC readout for space-based superconducting sensor arrays, in *Millimeter, Submillimeter, and Far-Infrared Detectors and Instrumentation for Astronomy XI* (SPIE, 2022), Vol. 12190, pp. 339–355
- [5] C. Liu, Z. Ahmed, S.W. Henderson, R. Herbst, L. Ruckman, Higher order nyquist zone sampling with rfsoc data converters for astronomical and high energy physics readout systems, arXiv preprint arXiv:2309.08640 (2023).
- [6] C. Liu, Z. Ahmed, S.W. Henderson, R. Herbst, L. Ruckman, T. Satterthwaite, Development of rfsoc-based direct sampling highly multiplexed microwave squid readout for future cmb and submillimeter surveys, arXiv preprint arXiv:2406.13156 (2024).
- [7] C. Liu, R. Herbst, B. Hong, L. Ruckman, E. Nanni, Direct rf sampling based llrf control system for c-band linear accelerator, Proc. IPAC'24 pp. 25–28 (2024).
- [8] C. Liu, R. Herbst, L. Ruckman, E. Nanni, Next generation LLRF control platform for compact c-band linear accelerator, in *EPJ Web of Conferences* (EDP Sciences, 2024), Vol. 315, p. 02008
- [9] C. Liu, L. Ruckman, R. Herbst, B. Hong, Z. Li, K. Kim, D. Amirari, R. Agustsson, J. Einstein-Curtis, M. Kilpatrick et al., A compact low-level rf control system for advanced concept compact electron linear accelerator, Review of Scientific Instruments 96 (2025).
- [10] C. Liu, L. Ruckman, R. Herbst, D. Palmer, V. Borzenets, A. Dhar, D. Amirari, R. Agustsson, R. Berry, E. Nanni, High-power test of a c-band linear accelerating structure with an rfsoc-based llrf system, Review of Scientific Instruments 96 (2025).
- [11] C. Liu, E. Snively, R. Herbst, K. Kim, E. Nanni, Next generation direct rf sampling llrf control and monitoring system for linear accelerators, arXiv preprint arXiv:2509.09905 (2025).
- [12] C. Liu, A. Dhar, E. Snively, M. Othman, R. Herbst, E.A. Nanni, Next generation llrf control and monitoring system for s-band linear accelerators, arXiv preprint arXiv:2505.22876 (2025).
- [13] E.A. Nanni, M. Breidenbach, Z. Li, C. Vernieri, F. Wang, G. White, M. Bai, S. Belomestnykh, P. Bhat, T. Barklow et al., Status and future plans for c3 r&d, Journal of Instrumentation 18, P09040 (2023).
- [14] M.B. Andorf, M. Bai, P. Bhat, V. Borzenets, M. Breidenbach, S. Dasu, A. Dhar, T.d. Pree, L. Gray, S. Gessner et al., Esppu input: C³ within the" linear collider vision", arXiv preprint arXiv:2503.20829 (2025).
- [15] Z. Farkas, H. Hogg, G. Loew, P.B. Wilson, SLED: A method of doubling SLAC's energy, in *Proc. Of 9th Int. Conf. On High Energy Accelerators, SLAC* (1974), p. 576